BEAM DYNAMICS SIMULATIONS OF THE NML PHOTOINJECTOR AT FERMILAB*

P. Piot[1,2], Y.-E Sun[1], and M. Church[1],
[1] Accelerator Physics Center, Fermi National Accelerator Laboratory, Batavia, IL, USA
[2] Department of Physics, Northern Illinois University, DeKalb, IL, USA

Abstract

Fermilab is currently constructing a superconducting RF (SRF) test linear accelerator at the New Muon Lab (NML). Besides testing SRF accelerating modules for ILC and Project-X, NML will also eventually support a variety of advanced accelerator R&D experiments. The NML incorporates a 40 MeV photoinjector capable of providing electron bunches with variable parameters. The photoinjector is based on the 1+1/2 cell DESY-type gun followed by two superconducting cavities. It also includes a magnetic bunch compressor, a round-to-flat beam transformer and a low-energy experimental area for beam physics experiments and beam diagnostics R&D. In this paper, we explore, via beam dynamics simulations, the performance of the photoinjector for different operating scenarios.

INTRODUCTION

A linear electron accelerator is under construction in the New Muon Lab building at Fermilab. The prime purpose of this accelerator is to operate, study and develop the superconducting cavities and asociated systems foreseen to be used in the International Linear Collider (ILC) [1] and for the relativistic section of Project-X [2]. For such a purpose, the electron beam current needs to mimic the ILC specifications, i.e. consist of 3000 3.2-nC bunches repeated at 3 MHz arranged as a 1-ms-duration macro-pulse with 5 Hz frequency. The ability to generate low transverse emittance and longitudinally compressed beam might open possibilities for the ILC R&D program as well as the conducting and extending the advanced accelerator physics program which Fermilab has been pursuing at the A0 photoinjector [3].

The photoinjector layout mimics the design philosophy of the FLASH injector of DESY [4]; see Fig. 1. The electron source includes a 1.3 GHz RF gun with a coaxial RF input coupler [5]. A high-quantum-efficiency cesium telluride (Cs_2Te) photocathode located on the back plate of the RF gun is illuminated by a uv photocathode drive laser thereby photoemitting high charge (several nC) bunches. For a conservative peak electric field of 40 MV/m, the beam's mean energy is approximately 5 MeV downstream of the gun. The gun is surrounded by two identical solenoids which, under nominal operation, are used to correct for the space-charge-induced correlated emittance growth. The solenoids configuration can also be used to control the magnetic field on the photocathode surface to generate angular-momentum-dominated beams. Downstream of the rf gun, two superconducting TESLA cavities accelerate the beam to 40 MeV approximately. The downstream beamline includes generic focusing elements, instrumentations along with a round-to-flat beam transformer composed of three skew quadrupoles, a magnetic bunch compressor and a dispersionless translating dogleg to direct the beam to an off-axis diagnotics/experimental area. The beam is then injected into a string of ILC modules and accelerated to its final energy (eventually up to $\sim$ 800 MeV) [6].

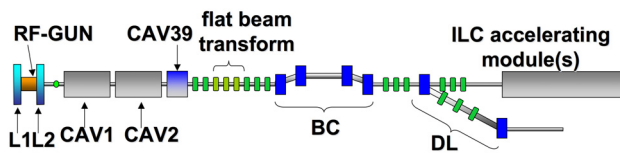

Figure 1: Overview of the low-energy injector. The legends are: "L1" "L2" solenoidal magnetic lenses, "CAV1" "CAV2" superconducting TESLA cavities, "CAV39" third harmonic ($f = 3.9$ GHz) superconducting cavity, "BC" magnetic bunch compressor chicane, "DL" dogleg. The green rectangles indicate the locations of quadrupoles.

BEAM GENERATION AND ACCELERATION

The photoinjector generates a high-charge beam and accelerates it to $\sim$ 40 MeV. In this process the operating parameters are tuned to minimize the transverse emittance. To have a low transverse emittance, the charge density can be reduced by using a long drive-laser pulse. The longitudinal emittance is increased during acceleration, due to quadratic correlations imparted to the longitudinal phase space by the 1.3-GHz rf-wave curvature. To reduce the longitudinal emittance, a 3rd order accelerating cavity (CAV39) is used on the decelerating phase to remove the longitudinal phase space curvature [7]. If CAV2 is operated off-crest, and CAV39 properly tuned, a linear chirp in the longitudinal phase space can be imparted to the bunch

* This work was supported by the Fermi Research Alliance, LLC under Contract No. DE-AC02-07CH11359 with the U.S. Department of Energy. P.P. was partially supported by the US Department of Energy under Contract No. DE-FG02-08ER41532 with Northern Illinois University.

which can then be compressed in the downstream magnetic bunch compressor chicane.

The initial conditions for the electron beam generation are determined by the photocathode drive laser parameters. For the present calculations, the uv laser is taken to be a Gaussian pulse with rms duration $\sigma_t = 3$ ps [8]. The small bandwidth supported by the laser system seeded by a Yb-doped fiber laser oscillator ($\Delta\lambda \sim 1$ Å) prevents sophisticated pulse shaping beyond pulse stacking. Four or eight 3-ps Gaussian pulses may be easily stacked to produce a quasi-uniform laser pulse thereby lowering the charge density. The operation with 1, 4 and 8 laser pulses is considered in the present paper. The initial normalized thermal emittance of the electron beam is related to the residual kinetic energy at emission and the rms beamsize σ on the photocathode via [9] $\varepsilon_n^{th} = \sigma[2E_{kin}/(3mc^2)]^{1/2}$ which gives $\varepsilon_n^{th}/\sigma \simeq 0.85$ μm.mm^{-1} for $E_{kin} = 0.55$ eV. This thermal emittance is included in the simulations presented.

The performance of the injector was explored for a variety of charges ranging from 20 pC to 3.2 nC with the three aforementioned laser shapes; see Fig. 2 (right). When several laser pulses are stacked together, the spacing between adjacent pulses needs to be chosen to minimize intensity modulations in the plateau region. Such temporal modulations would eventually transform into energy modulations (via modulation of the longitudinal space charge forces) which in turn could result in amplified density modulations downstream of a magnetic bunch compressor thereby leading to a klystron-like instability [10].

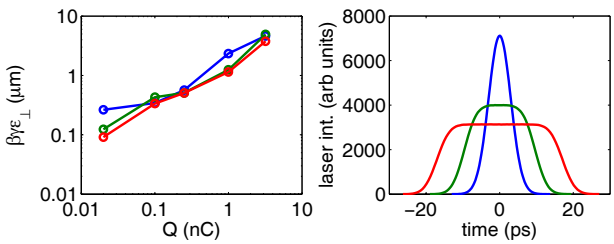

Figure 2: Optimized transverse emittances downstream of CAV39 (left) as a function of charge for the three pulse shapes (shown as different traces with color coding corresponding to the shape shown in the right plot).

A beam dynamics model of the injector was implemented in ASTRA [11] and a multi-objective genetic optimizer was used to optimize the transverse emittance downstream of CAV39 [12, 13]. To expedite the optimization process, ASTRA was run with 2000 macroparticles only, while 200k macroparticles were used to generate the data presented in this paper. The transverse emittance for the five considered charges and the three laser shapes are shown in Fig. 2. For $Q = 3.2$ nC the smallest achieved transverse emittance is $\varepsilon_\perp = 3.76$ μm while in the low charge operation ($Q = 20$ pC) an unprecedented low emittance value of $\varepsilon_\perp = 91.3$ nm has been reached in our simulations. This latter number could support the use of this

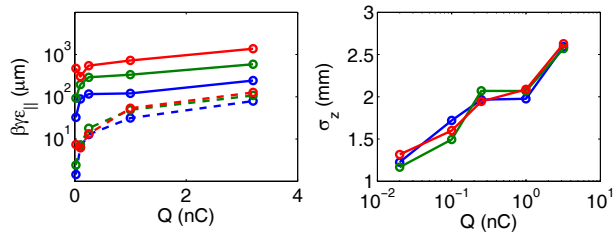

Figure 3: Longitudinal emittance (left) downstream as a function of charge for the three laser pulse shapes downstream of CAV2 (solid) and CAV39 (dashed line) and corresponding bunch length (right). The color coding follows Fig. 2 (right).

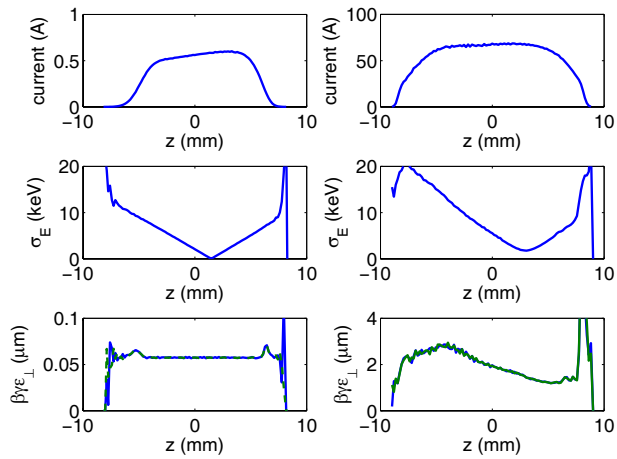

Figure 4: Current (top row), slice rms energy spread (middle row) and slice horizontal (blue) and vertical (green) emittance (bottom row) for $Q = 20$ pC (left column) and 3.2 nC (right column). For these calculations the beam was divided in 100 longitudinal slices. The head of the bunch corresponds to $z > 0$.

injector to produce very bright electron beams suitable, e.g. to drive an XFEL oscillator [14]. The corresponding longitudinal emittances and bunch length are shown in Fig. 3. The 3rd harmonic accelerating cavity that will eventually be installed downstream of the CAV2 cavity was not included in the present simulations but its impact on the longitudinal emittance [shown as dashed line in Fig. 3] was estimated by removing the second order curvature on the longitudinal phase spaces. Finally the slice parameters of these two cases of charge are shown in Fig. 4. The small slice energy spread supports the possible compression of the beam to sub-ps (possibly down to 10's fs) duration using a two-stage compression scheme. This would provide electron beams with performances comparable to state-of-the-art accelerators used to drive short wavelength FEL, or support advanced accelerator concept research.

TRANSPORT TO LINAC

Downstream of CAV39, the transport line includes a suite of diagnostics (including emittance and longitudinal phase space measurement), a round-to-flat beam transformer [15] and a magnetic chicane for bunch compression. The chicane dipoles have a nominal bending angle of $(+,-,-,+)18°$ leading to a longitudinal dispersion $R_{56} \simeq -0.19$ m. The correlation is imparted by CAV2 running off-crest. CAV1 is always run on crest for maximum energy gain. The large R_{56} provided by the chicane was driven by the need to be able to fully compress the electron bunch at 3.2 nC while maintaining a tolerable fractional momentum spread as required for tests related to the ILC program. In a later stage this compressor is foreseen to be part of a two stage compression scheme (the second compressor would be located downstream of three ILC cryomodules) and would therefore provide minor compression. The beamline is simulated with IMPACT-Z [16] by tracking the output phase space obtained with ASTRA. An example of beam sizes evolution throughout the injector transport line is shown in Fig. 5 for $Q = 3.2$ nC.

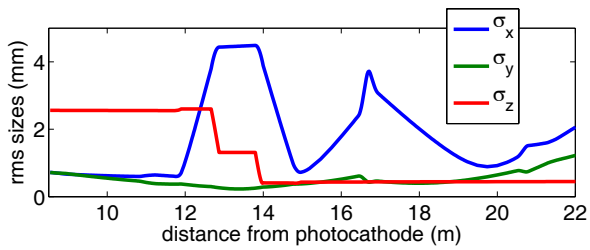

Figure 5: Evolution of the horizontal (blue), vertical (green) and longitudinal (red) rms sizes along the injector transport line. The bunch compressor extends from $\sim$ 12 to $\sim$ 15 m in this plot and the first ILC cryomodule starts at $\sim$ 22 m.

The compression of a 3.2 nC bunch yields a temporal distribution with a local charge concentration and long tail leading to an rms bunchlength of $\sim$ 400 μm; see middle row of Fig. 6. The transverse horizontal emittance grows by a factor ~ 5 according to IMPACT-Z and the corresponding horizontal phase space is highly bifurcated. The development of this phase space structures is driven by space charge effects: the inclusion of CSR effects in IMPACT-Z did not significantly change our results as depicted in Fig. 6. This mode of operation will initially be the only possible mode of operation of NML as CAV39 will not be available. Nevertheless tracking the distribution through the entire NML accelerator confirms that the achieved parameters are suitable to carry out experiments relevant to the ILC R&D program and support initial advanced accelerator concept experiments.

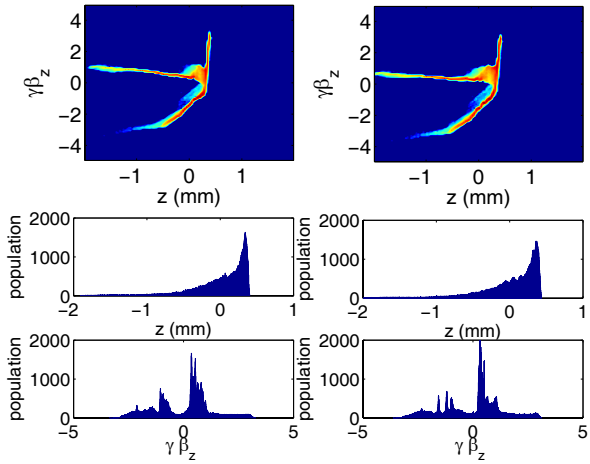

Figure 6: Longitudinal phase and associated projection downstream of a compressed 3.2-nC bunch taking into account space charge effects only (left) and space charge and CSR effects (right).

SUMMARY

We have demonstrated via numerical simulations that the photoinjector currently under construction at the NML facility will provide bright electron beams capable of supporting forefront beam physics research along with experiments dedicated to test novel acceleration or light source concepts. Further numerical simulations including wakefield effects and a self-consistent model of CSR are on-going. In addition the photoinjector will also be able to provide beams with partitioned transverse emittance, this mode of operation is yet to be investigated.

It is a pleasure to acknowledge Dr. J. Qiang from Berkeley for providing us with a copy of IMPACT-Z.

REFERENCES

[1] see http://www.linearcollider.org/rdr/.
[2] see http://projectx.fnal.gov/.
[3] see http://nicadd.niu.edu/fnpl.
[4] K. Flöttmann and P. Piot, Proc. EPAC02, 1798 (2002).
[5] B. Dwersteg *et al.*, *Nucl. Instr. and Meth.* **A 393**, 93 (1997).
[6] M. Church, *et al.*, Proc. PAC07, 2942 (2007).
[7] P. Piot, Proc. LINAC04. 528 (2004).
[8] J. Ruan, private communication (2010).
[9] K. Flöttmann, DESY report TESLA-FEL-1997-01 (1997).
[10] E. L. Saldin *et al.*, *Nucl. Instrum. Meth* **A 490**, 1 (2002).
[11] K. Flöttmann, http://www.desy.de/~mpyflo.
[12] I. Bazarov, and C.K. Sinclair *Phys. Rev. ST Accel. & Beams* **8**, 034202 (2005).
[13] M. Borland, H. Shang, private communication (2007).
[14] K.-J. Kim, *et al. Phys. Rev. Lett.* **100**, 244802 (2008).
[15] P. Piot, *et al.*, *Phys. Rev. ST Accel. Beams* **9**, 053501 (2006).
[16] J. Qiang, *at al.*, *J. Comp. Phys.* **163**, 434 (2000).